Spectral properties of the one-atom laser

Markus Löffler, Georg M. Meyer, and Herbert Walther
Max-Planck-Institut für Quantenoptik, Hans-Kopfermann-Strasse 1, D-85748 Garching, Germany
and Sektion Physik, Ludwig-Maximilians-Universität, München, Germany
(Received 27 December 1996)

The spectral properties of a two-level one-atom laser are investigated in a systematic way below and above threshold. For strong atom-field coupling several different regimes, depending on the pump rate, can be distinguished. The quantum properties of the one-atom laser lead to multipeaked output and fluorescence spectra. [S1050-2947(97)06705-X]

PACS number(s): 42.50.−p, 32.80.−t, 42.55.−f

I. INTRODUCTION

A single two-level atom strongly coupled to a resonator is one of the most fundamental systems to study the interaction of electromagnetic waves and matter at the quantum level. Corresponding experiments were first performed in the microwave regime [1] and later extended to the optical regime [2]. In the present paper we are interested in an atom permanently interacting with a resonator field at optical frequencies. Many aspects of similar systems have been investigated such as sub-Poissonian statistics and atom-field correlations [3], vacuum Rabi splitting [4–11], multipeaked spectra for a thermal cavity mode [12], and a spectrum with a multipeaked structure for an atom oscillating in a standing-wave cavity [13]. For a micromaser, multipeaked spectra have been predicted for both Poissonian [14,15] and regular [16,17] injection of the atoms.

More recently, one-atom systems have been studied that allow for the buildup of nonclassical laser light in the resonator mode. All of them have in common that a pump mechanism excites the atom and provides the energy to drive the system above threshold. For such a one-atom laser, details of the photon statistics [18–21] and some aspects of the field dynamics [19,20] have been studied. An experimental realization in the form of an ion-trap laser has been proposed [22]. The experimental setup envisioned is a single trapped ion that is permanently interacting with the light field.

So far, the spectral properties have been investigated mostly for the experimental situation of an atomic beam traversing a cavity, which is driven by a coherent field [7–11]. The response of the atom-cavity system to this external field has been studied. We, on the other hand, are interested in microscopic laser systems where an external incoherent pump excites the atom. In this case all photons in the resonator mode are generated by the atom itself. Such a laser system has the advantage of well-controlled conditions: there is only one atom present, so in contrast to the atomic beam experiments, we are not concerned with fluctuations of the number of atoms [9,11]. Also, the atom-field coupling strength can be fixed by localizing the atom within the Lamb-Dicke regime [23].

In this paper we investigate in detail the spectrum of a two-level one-atom laser in the strong-coupling regime below and above threshold. Between the parameter region that shows vacuum Rabi splitting and the laser region, a regime is found that is characterized by a spectrum with several peaks. In addition to the frequency of the vacuum Rabi oscillations, sum- and difference-frequency components are generated. By increasing the excitation rate, the system reaches a threshold and the spectrum changes drastically. In the laser region the output spectrum shows typical laser characteristics, and the fluorescence spectrum has the form of a Mollow triplet with a coherent peak at the center frequency.

This paper is organized as follows. In Sec. II we provide the master equation governing the dynamics of the one-atom laser. The definitions of the output and fluorescence spectra are given in Sec. III. There we also present an overview of the key features in the spectra for a large parameter range. The spectra below the laser threshold are discussed in detail in Sec. IV and those above threshold in Sec. V. Finally, Sec. VI gives a summary of the main results.

II. ONE-ATOM LASER

The system under investigation consists of a single two-level atom that serves as the active medium and is placed inside a resonator. Figure 1 shows a schematic representation of the setup. The coupling constant g describes the strength of the atom-field interaction. Atomic relaxation with the rate R_{AB} from the upper level $|\mathrm{A}\rangle$ to the lower level $|\mathrm{B}\rangle$ as well as cavity decay with the rate A are included. Since we are considering the two-level system as a model also for systems involving fast pumping via auxiliary levels, we allow the incoherent pump rate R_{BA} to be larger than R_{AB}. In the present paper we are primarily interested in the output spectrum $S_a(\omega)$ and the fluorescence spectrum $S_\sigma(\omega)$.

The dynamics of the atom-field density matrix ρ is governed by the master equation

$$\frac{\partial}{\partial t}\,\rho=\frac{1}{i\hbar}\,[H,\rho]+L_{\mathrm{atom}}\rho+L_{\mathrm{field}}\rho=\mathcal{L}\rho. \tag{1}$$

The resonant interaction between the atom and the resonator mode in the dipole and rotating-wave approximation and in the interaction picture is described by the Hamilton operator

$$H=i\hbar g(a^{\dagger}\sigma-a\sigma^{\dagger}), \tag{2}$$

where the photon creation and annihilation operators are $a^{\dagger}$ and a, respectively. The atomic raising and lowering operators are defined as

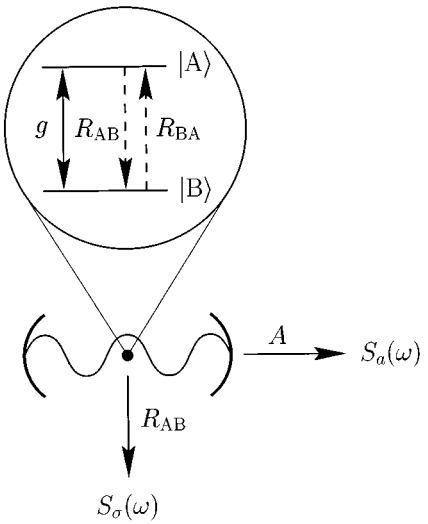

FIG. 1. Schematic representation of the setup. A single two-level atom is placed inside a resonator. The relevant parameters are the atom-field coupling strength g, the atomic relaxation and pump rates R_{AB} and R_{BA}, and the photon damping rate A. The output spectrum $S_a(\omega)$ and the fluorescence spectrum $S_\sigma(\omega)$ are considered.

$$\sigma^\dagger = |\mathrm{A}\rangle\langle\mathrm{B}|, \quad \sigma = |\mathrm{B}\rangle\langle\mathrm{A}|. \tag{3}$$

Atomic relaxations and incoherent pumping lead to nonunitary evolution given by

$$L_{\mathrm{atom}}\rho = -\frac{R_{AB}}{2}\,(\sigma^\dagger\sigma\rho + \rho\sigma^\dagger\sigma - 2\sigma\rho\sigma^\dagger) - \frac{R_{BA}}{2}\,(\sigma\sigma^\dagger\rho + \rho\sigma\sigma^\dagger - 2\sigma^\dagger\rho\sigma), \tag{4}$$

field damping is described by the Liouville operator

$$L_{\mathrm{field}}\rho = -\frac{A}{2}\,(\nu+1)(a^\dagger a\rho + \rho a^\dagger a - 2a\rho a^\dagger) - \frac{A}{2}\,\nu(aa^\dagger\rho + \rho aa^\dagger - 2a^\dagger\rho a) \tag{5}$$

with the photon damping rate A. As we are interested in the optical frequency domain, the number of thermal photons ν can be neglected in most cases.

III. OUTPUT AND FLUORESCENCE SPECTRUM

The dynamical properties, such as the spectrum, complete the picture of the field as drawn by the photon statistics and, thereby, provide additional physical insight. In order to illustrate that there is, of course, no one-to-one correspondence between the spectral properties and the photon statistics, we present in the Appendix four different systems with the same photon distribution, but with very different spectra.

Two kinds of spectra are relevant for the present system: the spectrum of the photons emitted through the cavity mirrors, here called the *output* spectrum $S_a(\omega)$, and the spectrum of the photons emitted out the sides of the cavity, here called the *fluorescence* spectrum $S_\sigma(\omega)$. They are defined as

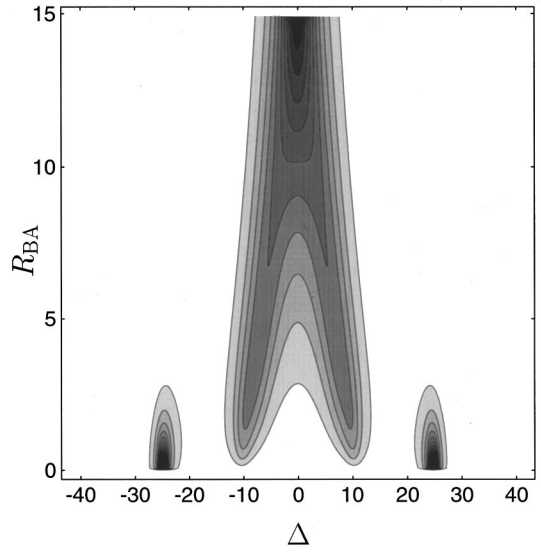

FIG. 2. Output spectrum $S_a(\omega)$ of the two-level one-atom laser. Darker areas correspond to larger values of $S_a(\omega)$. Between the regions showing vacuum Rabi splitting (small R_{BA}) and lasing (large R_{BA}) additional peaks occur. The parameters are $g=25$, $R_{AB}=1$, $\nu=0$ (in units of A).

$$S_a(\omega) = \int_0^\infty d\tau\, \cos(\omega\tau) g_a(\tau), \tag{6}$$

$$S_\sigma(\omega) = \int_0^\infty d\tau\, \cos(\omega\tau) g_\sigma(\tau) \tag{7}$$

with the normalized first-order correlation functions

$$g_a(\tau) = \lim_{t\to\infty} \frac{\langle a^\dagger(t+\tau)a(t)\rangle}{\langle a^\dagger(t)a(t)\rangle} = \frac{\mathrm{Tr}\{a^\dagger e^{\mathcal{L}\tau} a\rho^{(\mathrm{ss})}\}}{\mathrm{Tr}\{a^\dagger a\rho^{(\mathrm{ss})}\}}, \tag{8}$$

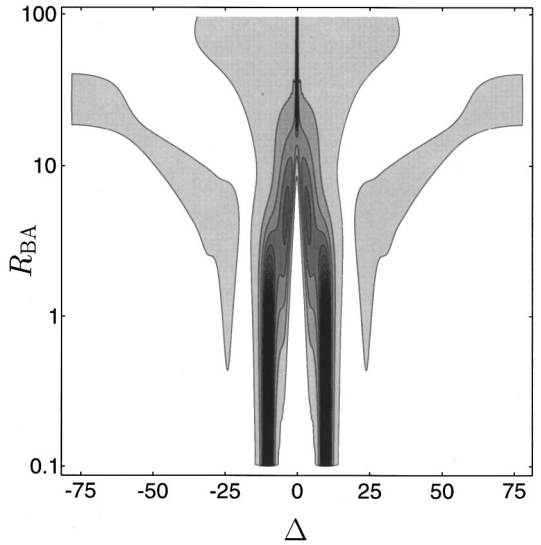

FIG. 3. Fluorescence spectrum $S_\sigma(\omega)$ of the two-level one-atom laser. Darker areas correspond to larger values of $S_\sigma(\omega)$. Vacuum Rabi splitting, multipeaked spectra, a Mollow triplet, and a narrow peak at center frequency are found for increasing R_{BA}. The parameters are $g=10$, $R_{AB}=1$, $\nu=0$ (in units of A).

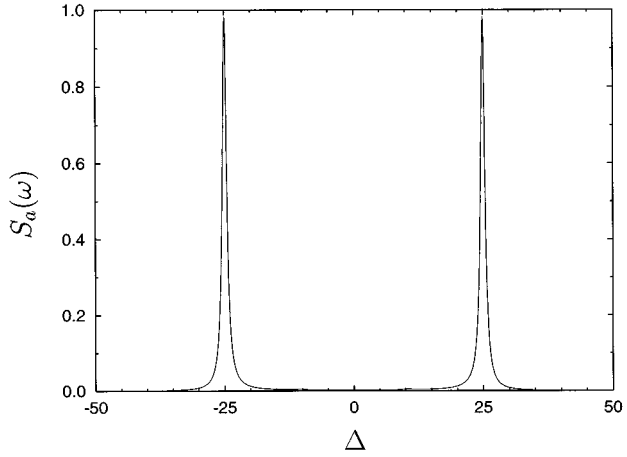

FIG. 4. Vacuum Rabi splitting in the output spectrum $S_a(\omega)$ for $R_{\mathrm{BA}}=0.01$. The other parameters are the same as in Fig. 2.

$$g_\sigma(\tau)=\lim_{t\to\infty}\frac{\langle\sigma^\dagger(t+\tau)\sigma(t)\rangle}{\langle\sigma^\dagger(t)\sigma(t)\rangle}=\frac{\mathrm{Tr}\{\sigma^\dagger e^{\mathcal{L}\tau}\sigma\rho^{(\mathrm{ss})}\}}{\mathrm{Tr}\{\sigma^\dagger\sigma\rho^{(\mathrm{ss})}\}}, \quad (9)$$

where $\rho^{(\mathrm{ss})}$ is the atom-field density matrix in the steady state. With this definition of the spectrum, we have

$$\frac{1}{\pi}\int_{-\infty}^{\infty}d\omega S_{a,\sigma}(\omega)=1. \quad (10)$$

The flux of output photons is given by $A\langle a^\dagger a\rangle$ and the flux of fluorescence photons by $R_{\mathrm{AB}}\langle\sigma^\dagger\sigma\rangle$.

The spectra presented in this paper are calculated numerically via Fourier transformation of the correlation functions. The latter are obtained by solving Eq. (1) in Fock representation for steady state and subsequent propagation in time according to Eqs. (8) and (9), respectively. The number of variables can be reduced by considering only the nonvanishing matrix elements, which couple among themselves.

Figures 2 and 3 show density plots of the output and fluorescence spectra as an overview for a wide range of values for the pump rate R_{BA}. For convenience of notation we define $\Delta=\omega-\omega_0$, where ω_0 is the frequency of the atomic transition and the resonator mode and ω is the frequency of the outcoming light. For increasing R_{BA}, regions with very different spectra can be distinguished. They are identified in the following paragraphs and discussed in detail in Sec. IV for the region below threshold and in Sec. V for the one above threshold.

The output spectrum $S_a(\omega)$ is illustrated in Fig. 2 for $g=25$, $R_{\mathrm{AB}}=1$, $R_{\mathrm{BA}}=0.01$. Throughout this paper all rates are given in units of the photon damping rate A. The spectrum consists of two narrow peaks at $\Delta=\pm g$ if R_{BA} is very small. This corresponds to the vacuum Rabi splitting. For larger pump rates, two more peaks arise in between the two former ones and become more and more pronounced. Their positions are at $\Delta=\pm g(\sqrt{2}-1)$. There are smaller peaks at $\Delta=\pm g(\sqrt{2}+1)$, which are not shown in Fig. 2. The origin of these difference- and sum-frequency peaks is discussed in Sec. IV. Eventually, for even larger pump rates R_{BA}, lasing takes place and a large peak at $\Delta=0$ occurs.

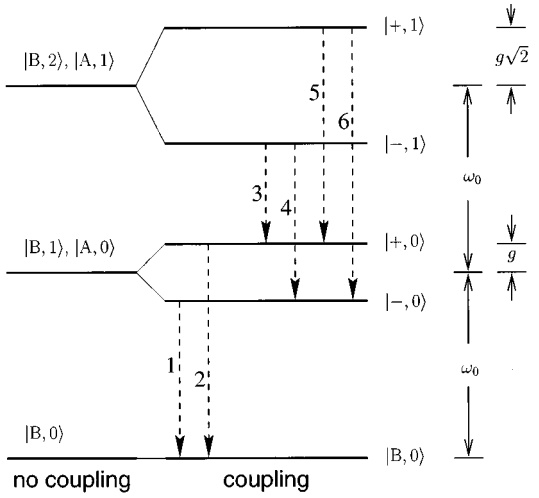

FIG. 5. Dressed-state picture illustrating the origin of the sum- and difference-frequency peaks. The transitions (1) and (2) correspond to the vacuum Rabi splitting peaks at $\omega_0\pm g$. If the mean photon number is of the order of or larger than 1, a considerable part of the population is in the dressed states $|\pm,1\rangle$ and the transitions (3)–(6) with the frequencies $\omega_0\pm g(\sqrt{2}\pm1)$ are relevant.

A similar but somewhat different behavior can be found in the fluorescence spectrum $S_\sigma(\omega)$, as plotted in Fig. 3 for $g=10$. Again the pump rate is shown on the y axis; here the scale is logarithmic in order to cover a larger range. For very small R_{BA}, the fluorescence and the output spectrum nearly look the same, both showing vacuum Rabi splitting. Around $R_{\mathrm{BA}}=1$, a multipeaked spectrum with peaks at the sum and difference frequencies $\Delta=\pm g(\sqrt{2}\pm1)$ can be found as in the output spectrum. In the fluorescence spectrum, however, the peaks at the sum frequency are more pronounced. Similar fluorescence spectra have been obtained in Ref. [12] for a thermal cavity mode. For larger pump rates a Mollow spectrum [24] arises. The sidebands are pushed to larger frequencies by an increasing pump rate. At the center frequency there is a dip for values of R_{BA} up to about 10, then a coherent peak on top of the Mollow triplet shows up. The origin of this peak is coherent scattering of the generated laser light by the atom. For even larger pump rates, the laser reaches a second threshold and goes out due to self-quenching, as the incoherent pump destroys the coherence on the laser transition. The onset of this behavior can be seen in Fig. 3 around $R_{\mathrm{BA}}=100$.

IV. SUM- AND DIFFERENCE-FREQUENCY GENERATION

Figure 4 shows a plot of the output spectrum $S_a(\omega)$ in the parameter regime, where the vacuum Rabi splitting is dominant. The fluorescence spectrum is very similar for these parameters. The physical reason for these peaks can be understood in a dressed-state picture such as Fig. 5. If there is no coupling, the states $|\mathrm{B},n\rangle$ and $|\mathrm{A},n-1\rangle$ are degenerate. With the atom-field coupling present, the degeneracy is removed, leading to an energy difference of $2\hbar g\sqrt{n}$ between the dressed states $|\pm,n\rangle=(|\mathrm{B},n\rangle\pm|\mathrm{A},n-1\rangle)/\sqrt{2}$. As these states are the energy eigenstates of the system, the frequency differences between them show up in both the fluorescence and the output spectrum. For a very small pump rate R_{BA},

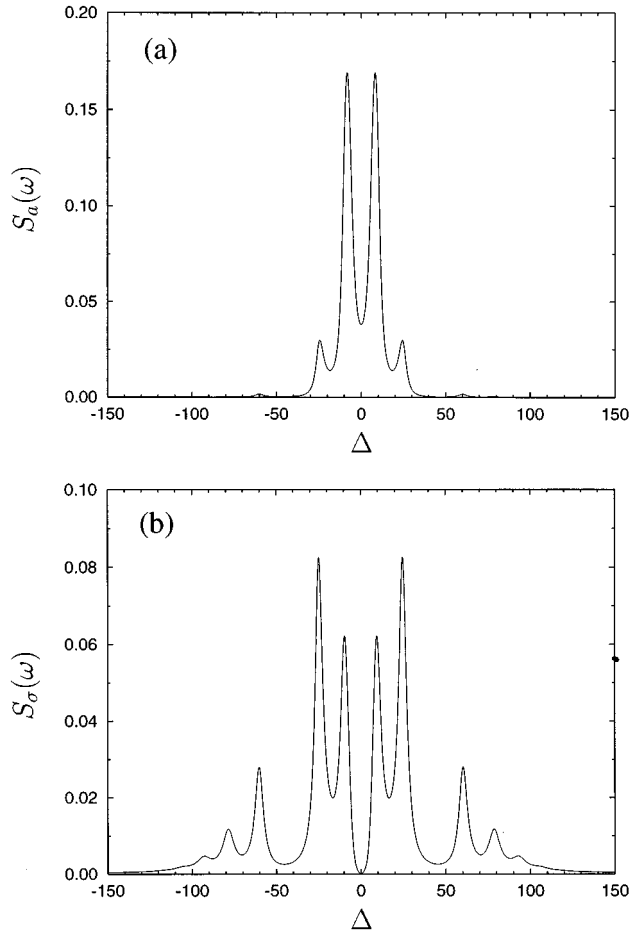

FIG. 6. Sum- and difference-frequency generation in (a) the output spectrum $S_a(\omega)$ and (b) the fluorescence spectrum $S_\sigma(\omega)$. The pump rate is $R_{\mathrm{BA}}=3$, the other parameters are the same as in Fig. 2.

the mean photon number is much smaller than 1. Therefore, only the lowest steps of the dressed-state ladder are occupied. There are two possible transitions to the ground state, namely, (1) $|-,0\rangle\rightarrow|\mathrm{B},0\rangle$ and (2) $|+,0\rangle\rightarrow|\mathrm{B},0\rangle$ with the frequencies $\omega_0\pm g$, leading to the vacuum Rabi splitting. The transition rates in such a dressed-atom picture are determined partly by the atomic relaxation rate R_{BA}, partly by the photon damping rate A. These processes generate output and fluorescence photons, respectively. As pointed out in Ref. [8], the vacuum Rabi splitting can also be understood classically in terms of a linear-dispersion theory.

Figure 6 shows plots of (a) the output and (b) the fluorescence spectrum for a larger pump rate. Compared to Fig. 4, additional peaks are found. In contrast to the vacuum Rabi splitting, the origin of these peaks is intrinsically connected to the quantum nature of the light field and cannot be explained in terms of a classical theory. To illuminate the physical mechanism leading to peaks at the sum and difference frequencies $\Delta=g(\sqrt{n+1}\pm\sqrt{n})$, it is again useful to consider the dressed-state picture of the atom-cavity system in Fig. 5. There are four transitions between the states $|\pm,n\rangle$ and $|\pm,n-1\rangle$. In Fig. 5 they are drawn for $n=1$ and labeled (3)–(6). The corresponding frequencies are $\omega_0\pm g(\sqrt{2}\pm1)$, as can be seen from the schematic.

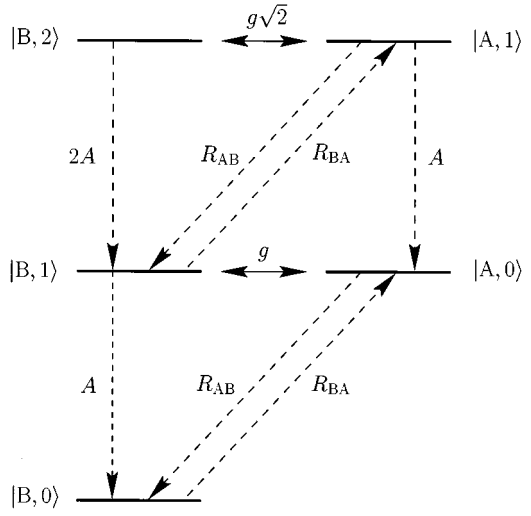

FIG. 7. The states $|\mathrm{B},n\rangle$ and $|\mathrm{A},n-1\rangle$ ($n\geqslant1$) form a ladder of ''Rabi oscillators,'' which are coupled by decay (R_{AB}, A) and pumping (R_{BA}).

For a very weak pump R_{BA}, only the lowest levels $|\mathrm{B},0\rangle$, $|-,0\rangle$, and $|+,0\rangle$ are occupied, therefore only the transitions (1) and (2) can be seen in the spectrum. With increasing R_{BA} more of the higher levels are occupied and more peaks arise. In Ref. [12] similar spectra have been found. There the occupation of higher dressed states is due to the presence of thermal photons. As we are primarily interested in the optical domain, the number of thermal photons is close to zero for all practical purposes. Instead, we have introduced an incoherent pump to excite higher dressed states.

The dressed-state considerations made above explain the approximate position of the peaks but not their spectral width. If there were no pumping present, the positions of the levels in Fig. 5 would yield the exact positions of the peaks. With a nonvanishing pump rate, the peaks are not only broadened, but also shifted. Figure 7 illustrates the explanation for this effect. The pairs of levels $|\mathrm{B},n\rangle$ and $|\mathrm{A},n-1\rangle$ ($n\geqslant1$) form a ladder of oscillators with the frequencies $g\sqrt{n}$. Incoherent pumping (R_{BA}), atomic relaxation (R_{AB}), and photon damping (A) couple the rungs of this ladder; therefore the oscillation is driven and damped. Very much as in classical mechanics, this leads to a shift and broadening of the resonances. Atomic relaxation and incoherent pumping are the same for all rungs, whereas the photon damping increases with n and the coupling strength is proportional to $\sqrt{n}$. This subtlety has to be taken into account and one expects that the effective shifts and widths of the resonances are different for different n. Of course, it is not the dynamics of the populations (as Fig. 7 might suggest) that governs the spectrum but the dynamics of the first off-diagonal of the field density matrix. The picture of driven, damped ''Rabi oscillators,'' however, illustrates the mechanism of sum- and difference-frequency generation and the broadening and shifts of the corresponding peaks.

In order to calculate the exact positions and widths, we analyze the eigenvalues governing the output spectrum. To that end we use Eq. (8), define

$$\tilde{\rho} = a\rho^{(ss)}, \tag{11}$$

expand $\tilde{\rho}$ in terms of the atomic levels $|A\rangle$, $|B\rangle$ and photon number states $|n\rangle$, $|n'\rangle$,

$$\tilde{\rho} = \sum_{L,L'} \sum_{n,n'} \tilde{\rho}_{LL'}^{nn'} |L,n\rangle\langle L,n'|, \tag{12}$$

and write the expansion coefficients as a vector:

$$v = (\tilde{\rho}_{BA}^{0,0}, \tilde{\rho}_{BB}^{0,1}, \tilde{\rho}_{AA}^{0,1}, \tilde{\rho}_{AB}^{0,2}, \tilde{\rho}_{BA}^{1,1}, \tilde{\rho}_{BB}^{1,2}, \tilde{\rho}_{AA}^{1,2}, \tilde{\rho}_{AB}^{1,3}, \tilde{\rho}_{BA}^{2,2}, \tilde{\rho}_{BB}^{2,3}, \dots)^T. \tag{13}$$

The time evolution of v is governed, according to Eq. (1), by

$$\frac{\partial}{\partial t} v = Mv \tag{14}$$

with

$$M = \begin{pmatrix} B_0 & C_0 & 0 & 0 & 0 & \\ A_0 & B_1 & C_1 & 0 & 0 & \\ 0 & A_1 & B_2 & C_2 & 0 & \\ 0 & 0 & A_2 & B_3 & C_3 & \\ & & & \ddots & \ddots & \ddots \end{pmatrix}, \tag{15}$$

$$A_0 = \begin{pmatrix} 0 & R_{BA} \\ 0 & 0 \\ 0 & 0 \\ 0 & 0 \end{pmatrix}, \quad B_0 = \begin{pmatrix} -\gamma_{AB} & -g \\ g & -R_{BA} - A/2 \end{pmatrix}, \quad C_0 = \begin{pmatrix} A & 0 \\ 0 & A\sqrt{2} \end{pmatrix}, \tag{16}$$

$$A_N = \begin{pmatrix} 0 & 0 & 0 & R_{BA} \\ 0 & 0 & 0 & 0 \\ 0 & 0 & 0 & 0 \\ 0 & 0 & 0 & 0 \end{pmatrix}, \quad C_N = \begin{pmatrix} \sqrt{N(N+1)} & 0 & 0 & 0 \\ 0 & \sqrt{N(N+2)} & 0 & 0 \\ 0 & 0 & A(N+1) & 0 \\ R_{AB} & 0 & 0 & A\sqrt{(N+1)(N+2)} \end{pmatrix}, \tag{17}$$

and

$$B_N = \begin{pmatrix} -R_{AB} - A(N-1/2) & -g\sqrt{N+1} & -g\sqrt{N} & 0 \\ g\sqrt{N+1} & -\gamma_{AB} - AN & 0 & -g\sqrt{N} \\ g\sqrt{N} & 0 & -\gamma_{AB} - AN & -g\sqrt{N+1} \\ 0 & g\sqrt{N} & g\sqrt{N+1} & -R_{BA} - A(N+1/2) \end{pmatrix}, \tag{18}$$

with $\gamma_{AB} = (R_{AB} + R_{BA})/2$. To calculate the eigenvalues for the fluorescence spectrum, one can define

$$\tilde{\rho} = \sigma\rho^{(ss)}, \tag{19}$$

instead of Eq. (11). This leads to the same matrix equation (14) as for the output spectrum.

In Fig. 8 the imaginary parts of the most important eigenvalues of M are plotted as a function of R_{BA}. They determine the positions of the different peaks. The dashed line represents the position expected from the dressed-state picture of Fig. 5: (a) $g(\sqrt{2}-1)$, (b) g, and (c) $g(\sqrt{2}+1)$. For very small pump rates R_{BA}, they coincide with the exact values. With increasing pump rate, there is an increasing deviation from this value, as the pump process leads to level shifts of the dressed states towards lower frequencies. These shifts are less pronounced for the vacuum Rabi splitting (b) than for the higher-order peaks (a) and (c). In Fig. 9 the real parts of the same eigenvalues are plotted as a function of R_{BA}. They determine the widths of the different peaks. The widths of all peaks increase linearly with R_{BA}. The vacuum Rabi splitting is most sensitive to this broadening.

For very small pump rates ($R_{BA} \to 0$), the eigenvalues of M [Eq. (15)] are given by the eigenvalues of B_N and can be obtained analytically. In particular, the positions and widths of the vacuum Rabi peaks are given by the eigenvalues of the (2×2)-matrix B_0:

$$\lambda_{1,2} = -\frac{R_{AB} + A}{4} \pm i\sqrt{g^2 - \tfrac{1}{4}(R_{AB} - A)^2}. \tag{20}$$

Therefore, vacuum Rabi splitting only occurs when $g > |R_{AB} - A|/2$. The width is always $(R_{AB} + A)/4$ independent of g. As has been pointed out in Ref. [6], this linewidth is much smaller than the one in free space.

For the lowest-order sum- and difference-frequency peaks, we get from the (4×4)-matrix B_1

$$\lambda_{3,4,5,6} = -\frac{R_{AB} + 2A}{2} \pm i\left[3g^2 - \frac{1}{8}(R_{AB} - A)^2 \pm \sqrt{[3g^2 - \tfrac{1}{8}(R_{AB} - A)^2]^2 - g^2}\right]^{1/2}. \tag{21}$$

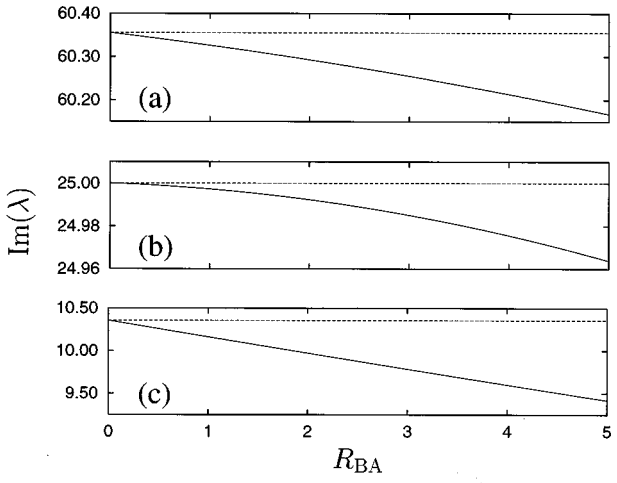

FIG. 8. Position of the most important peaks as given by the imaginary part of the eigenvalues governing the spectrum as a function of R_{BA}. The dashed lines correspond to (a) $g(\sqrt{2}+1)$, (b) g, and (c) $g(\sqrt{2}-1)$, respectively. The parameters are the same as in Fig. 2.

If g is not too small, the width of these four peaks is $A+R_{AB}/2$, independent of g.

For the special case $A=R_{AB}$, Eqs. (20) and (21) can be simplified to $\lambda_{1,2}=-A/4\pm ig$ and $\lambda_{3,4,5,6}=-3A/2 \pm ig(\sqrt{2}\pm 1)$, and the peaks are exactly at the positions, which are suggested by the simple dressed-state picture (Fig. 5). As the analysis for the fluorescence spectrum involves the same matrix equation (14), the results for the position and width of the fluorescence peaks are the same as for the output spectrum.

V. LASING AND MOLLOW SPECTRUM

With an increasing pump rate R_{BA}, a region occurs where the mean photon number increases linearly and the intensity fluctuations go through a maximum. As discussed in Refs. [20, 21], this can be interpreted as a threshold. Above this threshold laser light with nearly Poissonian statistics is generated. It has been pointed out in Ref. [19] that the output spectrum in the laser region has a Lorentzian shape and its width decreases with increasing intensity. We here study the output spectrum in a more systematic way, and in addition the fluorescence spectrum.

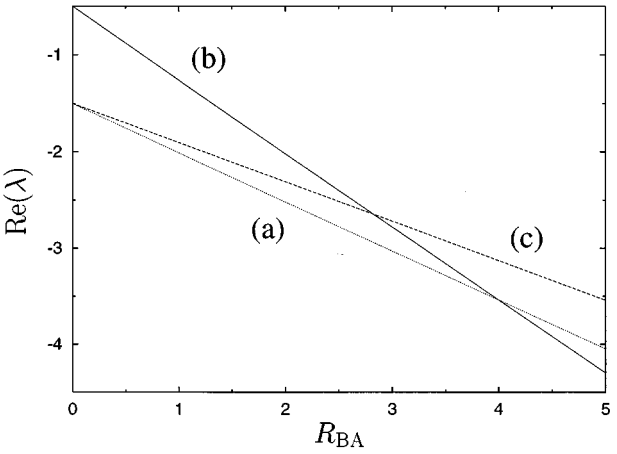

FIG. 9. Width of the most important peaks as given by the negative of the real parts of the eigenvalues governing the spectrum. The peaks are approximately at (a) $\Delta=g(\sqrt{2}+1)$, (b) $\Delta=g$, and (c) $\Delta=g(\sqrt{2}-1)$. The parameters are the same as in Fig. 2.

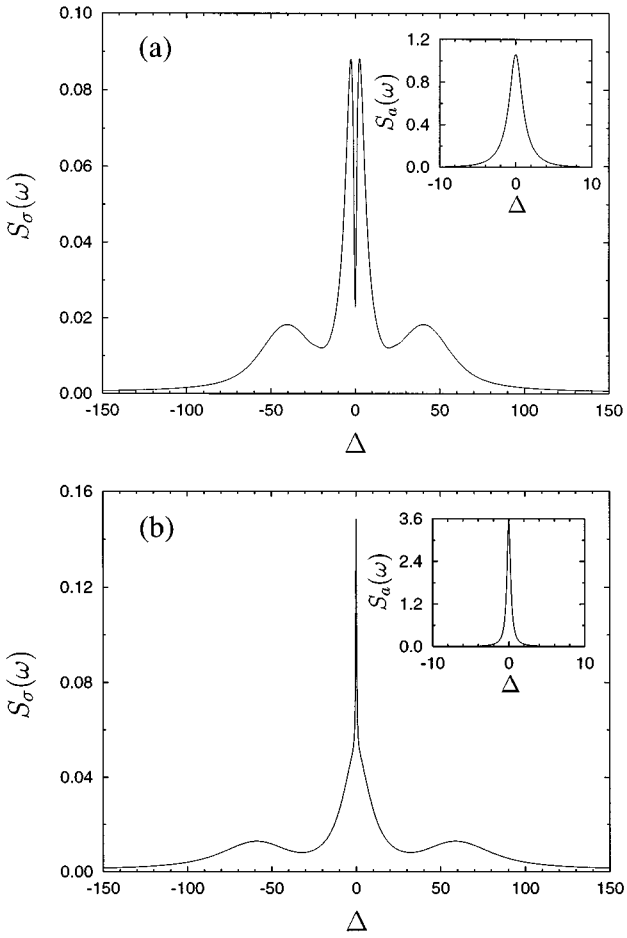

FIG. 10. Fluorescence spectrum $S_\sigma(\omega)$ for (a) $R_{BA}=10$ and (b) $R_{BA}=20$; the other parameters are the same as in Fig. 3. The insets show the corresponding output spectra.

In Fig. 10(a) the fluorescence spectrum $S_\sigma(\omega)$ is plotted. It shows a Mollow-like spectrum with a dip at center frequency. The dip has the width of the output spectrum, shown in the inset of Fig. 10(a), and can be explained as follows: the photons close to resonance are mostly emitted into the resonant mode of the cavity, therefore there is a hole in the fluorescence spectrum. This is very different from the situation described in Ref. [11], where a dip in the transmission is found together with a single peak in the fluorescence. There the coupling is weak and the system is in the bad-cavity regime ($A \gg R_{AB}$); photons at the center frequency are mainly coherently scattered and contribute to the fluorescence, while they are missing in the transmitted light.

If the pump rate is increased, the dip vanishes and eventually a narrow coherent peak arises on top of the Mollow spectrum [24] as shown in Fig. 10(b). This behavior is due to the fact that with increasing pump rate the number of photons in the cavity mode increases. As there are now enough resonant photons, the hole in the fluorescence spectrum vanishes, and for even higher photon numbers coherent scattering of resonant photons leads to a coherent peak. The width

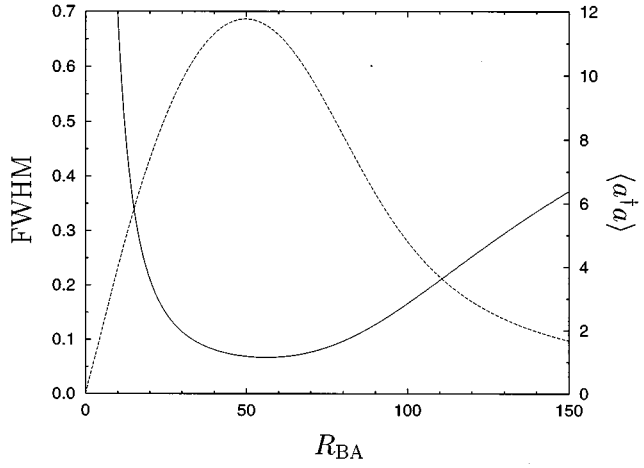

FIG. 11. FWHM of the coherent peak in the fluorescence spectrum or of the output spectrum (solid) and mean photon number (dashed). The parameters are $g=5$, $R_{\mathrm{AB}}=1$, $\nu=0$ (in units of A).

of this coherent peak in the fluorescence spectrum is the same as the width of the output spectrum.

The variation of the width as a function of R_{BA} together with the mean photon number $\langle a^\dagger a \rangle$ is shown in Fig. 11. The numerical results for the widths of the two kinds of spectra agree within the thickness of the curve. It can be seen that the spectrum narrows in the lasing region, where the mean photon number has its maximum. For $R_{\mathrm{BA}} \simeq 60$, the full width at half maximum (FWHM) is about 0.1. This is 1/10 of the cavity decay rate A and the atomic relaxation rate R_{BA}.

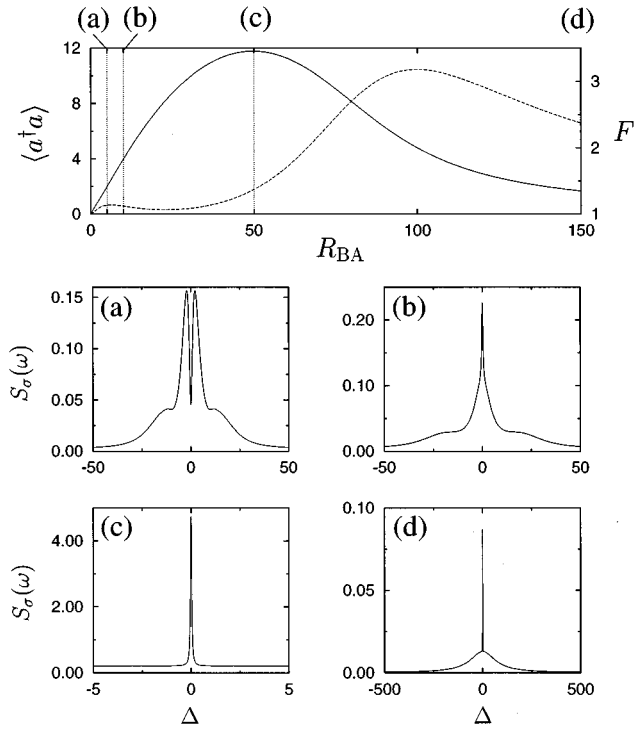

FIG. 12. Fluorescence spectrum for different pump rates $R_{\mathrm{BA}}=5$ (a), 10 (b), 50 (c), and 150 (d). The upper plot shows the corresponding mean photon number $\langle a^\dagger a \rangle$ and Fano factor F. The other parameters are the same as in Fig. 11.

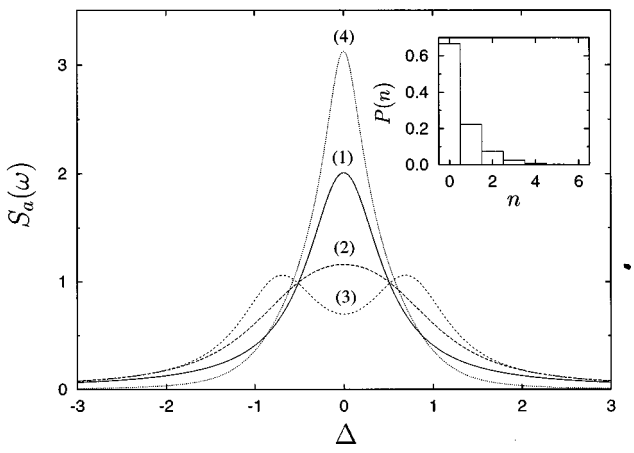

FIG. 13. Different spectra for the same photon distribution, which is shown in the inset. The parameters are given in Table I.

If the incoherent pump rate is increased further, the atomic coherence on the laser transition is destroyed and a second threshold is reached (self-quenching). The mean photon number decreases and the output spectrum broadens, as well as the coherent peak in the fluorescence spectrum, as can be seen in Fig. 11.

Figure 12 shows typical plots of the fluorescence spectrum for each excitation region together with the mean photon number $\langle a^\dagger a \rangle$ and the Fano factor $F=\langle (a^\dagger a - \langle a^\dagger a \rangle)^2 \rangle / \langle a^\dagger a \rangle$, which measures the intensity fluctuations. The parameters are the same as in Fig. 11. Around the first threshold the spectrum looks like a Mollow spectrum with a dip at center frequency, as shown in Fig. 12(a). Shortly above this threshold, a coherent peak shows up instead of the dip (b). In the region, where lasing is strongest, this coherent peak dominates the fluorescence spectrum entirely (c). If the pumping is so strong that self-quenching takes place, the photon number in the laser mode decreases and the coherent peak becomes smaller compared to the broad incoherent background. In this region the incoherent peaks are broadened so much that the sidebands of the triplet are not resolved (d).

A physical explanation of the Mollow spectrum can be given with the help of the dressed-state picture of Fig. 5. In the laser region, many rungs of the dressed-state ladder are occupied and the contributions of several decay channels overlap. With increasing photon number n, the energy splitting of neighboring dressed-state pairs differs only by a small amount. For the relevant photon numbers n, it can be approximated by $2\hbar g\sqrt{\langle a^\dagger a \rangle}$, which determines the position of the sideband peaks. To obtain the widths and heights of the three Mollow peaks, one has to take into account the rates for

TABLE I. Parameters for Fig. 13. No entry indicates that the corresponding parameter could have any value.

Plot	g	A	ν	R_{AB}	R_{BA}
(1)	0	1	0.5		
(2)	1	1	0.5	1.5	0.5
(3)	1	1	0.5	0	0
(4)	1	0		1.5	0.5

cavity damping, atomic decay and pumping as well as quantum interferences between different decay channels [25].

VI. SUMMARY

We have systematically investigated the output and fluorescence spectrum of a two-level one-atom laser below and above threshold. For small pump rates, the quantum nature of the atom-field interaction leads to several peaks in both kinds of spectra, corresponding to transitions between dressed states. We have discussed the positions and widths of these peaks under the influence of pumping and relaxation. Larger pump rates drive the system above the laser threshold, leading to a line narrowing in the output spectrum. The fluorescence spectrum close to threshold has the form of a Mollow triplet with a dip at the center frequency. Above threshold a coherent peak shows up that is due to Rayleigh scattering of photons from the generated laser field. In the parameter regime where the lasing is strongest, this coherent peak dominates the fluorescence spectrum. For very large pump rates, together with the mean photon number the coherent peak decreases and the peaks of the Mollow triplet merge into a broad incoherent background. While the vacuum Rabi splitting has been demonstrated experimentally in atomic beam experiments, the other interesting features of the spectra are still to be seen.

ACKNOWLEDGMENTS

The authors would like to thank H.-J. Briegel and B.-G. Englert for valuable discussions.

APPENDIX: DIFFERENT SPECTRA FOR THE SAME PHOTON DISTRIBUTION

It is possible to obtain very different output spectra for different systems although their photon distribution $P(n)$ is the same. This is illustrated in Fig. 13 for a thermal distribution. In Table I the parameters are listed, which lead to a thermal distribution with $\langle a^{\dagger}a\rangle = 0.5$ in the steady state. Field damping can be described by the coupling of the cavity mode to a reservoir with the temperature $T_{\text{field}} = -\hbar\omega_0/\{k_B \ln[\nu/(\nu+1)]\}$, where ν is the number of thermal photons. Correspondingly, atomic relaxations and incoherent pumping can be thought of as originating from the coupling to a reservoir with the temperature $T_{\text{atom}} = -\hbar\omega_0/\{k_B \ln[R_{\text{BA}}/R_{\text{AB}}]\}$.

The different possibilities correspond to the following situations: (1) No atom is present or the atom does not couple to the field ($g=0$). The field is damped according to a heat bath at temperature $T_{\text{field}}=T_0$. (2) The atom couples to the field. The heat bath corresponding to the field damping has the same temperature as the reservoir leading to atomic relaxation: $T_{\text{atom}}=T_{\text{field}}=T_0$. In this case $\nu/(\nu+1)=R_{\text{BA}}/R_{\text{AB}}$. (3) The atom couples to the field, no atomic relaxation is present. The heat bath corresponding to the field damping has the temperature $T_{\text{field}}=T_0$. (4) The atom couples to the field, no field relaxation is present. The reservoir corresponding to the atomic relaxation has the temperature $T_{\text{atom}}=T_0$. This example shows that systems with the same statistical steady-state properties can have very different dynamical properties such as the output spectrum.

[1] For a review, see G. Raithel, C. Wagner, H. Walther, L. M. Narducci, and M. O. Scully, in *Cavity Quantum Electrodynamics*, edited by P. R. Berman (Academic Press, Boston, 1994), p. 57.
[2] A review is given by H. J. Kimble, in *Cavity Quantum Electrodynamics*, edited by P. R. Berman (Academic Press, Boston, 1994), p. 203.
[3] G. S. Agarwal and S. Dutta Gupta, Phys. Rev. A **42**, 1737 (1990).
[4] J. J. Sanchez-Mondragon, N. B. Narozhny, and J. H. Eberly, Phys. Rev. Lett. **51**, 550 (1983).
[5] G. S. Agarwal, Phys. Rev. Lett. **53**, 1732 (1984).
[6] H. J. Carmichael, R. J. Brecha, M. G. Raizen, H. J. Kimble, and P. R. Rice, Phys. Rev. A **40**, 5516 (1989).
[7] M. G. Raizen, R. J. Thompson, R. J. Brecha, H. J. Kimble, and H. J. Carmichael, Phys. Rev. Lett. **63**, 240 (1989).
[8] Y. Zhu, D. J. Gauthier, S. E. Morin, Q. Wu, H. J. Carmichael, and T. W. Mossberg, Phys. Rev. Lett. **64**, 2499 (1990).
[9] F. Bernardot, P. Nussenzveig, M. Brune, J. M. Raimond, and S. Haroche, Europhys. Lett. **17**, 33 (1992).
[10] R. J. Thompson, G. Rempe, and H. J. Kimble, Phys. Rev. Lett. **68**, 1132 (1992).
[11] J. J. Childs, K. An, M. S. Otteson, R. R. Dasari, and M. S. Feld, Phys. Rev. Lett. **77**, 2901 (1996).
[12] J. I. Cirac, H. Ritsch, and P. Zoller, Phys. Rev. A **44**, 4541 (1991).
[13] W. Ren, J. D. Cresser, and H. J. Carmichael, Phys. Rev. A **46**, 7162 (1992).
[14] N. Lu, Phys. Rev. Lett. **70**, 912 (1993).
[15] K. Vogel, W. P. Schleich, M. O. Scully, and H. Walther, Phys. Rev. A **48**, 813 (1993).
[16] H.-J. Briegel, B.-G. Englert, C. Ginzel, and A. Schenzle, Phys. Rev. A **49**, 5019 (1994); H.-J. Briegel, B.-G. Englert, and M. O. Scully, *ibid.* **54**, 3603 (1996).
[17] J. A. Bergou, Quantum Semiclass. Opt. **7**, 327 (1995).
[18] Y. Mu and C. M. Savage, Phys. Rev. A **46**, 5944 (1992).
[19] C. Ginzel, H.-J. Briegel, U. Martini, B.-G. Englert, and A. Schenzle, Phys. Rev. A **48**, 732 (1993).
[20] T. Pellizzari and H. Ritsch, J. Mod. Opt. **41**, 609 (1994).
[21] H.-J. Briegel, G. M. Meyer, and B.-G. Englert, Phys. Rev. A **53**, 1143 (1996); Europhys. Lett. **33**, 515 (1996).
[22] G. M. Meyer, H.-J. Briegel, and H. Walther, Europhys. Lett. **37**, 317 (1997).
[23] J. T. Höffges, H. W. Baldauf, T. Eichler, S. R. Helmfrid, and H. Walther, Opt. Commun. **133**, 170 (1997).
[24] B. R. Mollow, Phys. Rev. **188**, 1969 (1969).
[25] C. Cohen-Tannoudji, in *Frontiers in Laser Spectroscopy*, edited by R. Balian, S. Haroche, and S. Liberman (North-Holland, Amsterdam, 1977), Vol. 1, p. 3.